SUPPORTING INFORMATION FOR

Photoinduced Magnetism in Core-Shell Prussian Blue Analog Heterostructures of $K_jNi_k[Cr(CN)_6]_l \cdot nH_2O$ with $Rb_aCo_b[Fe(CN)_6]_c \cdot mH_2O$

Matthieu F. Dumont [a], Elisabeth S. Knowles [b], Amandine Guiet [a], Daniel M. Pajerowski [b], Ariel Gomez [c], Stefan W. Kycia [c], Mark W. Meisel [b] and Daniel R. Talham [a]

[a] Department of Chemistry, University of Florida, Gainesville, FL 32611-7200, USA.

[b] Department of Physics and the National High Magnetic Field Laboratory, University of Florida, Gainesville, FL 32611-8440, USA.

[c] Department of Physics, University of Guelph, Guelph, ON, N1G 2W1, Canada

This Supporting Information contains: **(1)** schematic of heterostructured particles along with a calculation of the expected EDS profile based on the particle architecture, as well as the EDS results for the individual metals in **ABA** and **BAB** heterostructures; **(2)** the temporal evolution of the magnetic response for a **BA** heterostructure during irradiation at 40 K and high field magnetization at 2 K; **(3)** a description of the synthesis protocol and procedures to determine the relative molar extinction coefficients for Co^{III}-NC-Fe^{II} (LS), Co^{II}-NC-Fe^{II} (reduced) and Ni^{II}-NC-Cr^{III} pairs; **(4)** FT-IR spectra for the RbCoFe core (**B**), RbCoFe/KNiCr (**BA**), RbCoFe/KNiCr/RbCoFe (**BAB**), KNiCr core (**A**), KNiCr/RbCoFe (**AB**), and KNiCr/RbCoFe/KNiCr (**ABA**) particles; **(5)** Magnetic susceptibility, χ, as a function of temperature for **BAB**, **AB**, and **ABA** particles; **(6)** TEM images following each step in the preparation of core/shell/shell heterostructures.

1. Heterostructured particles scheme and EDS.

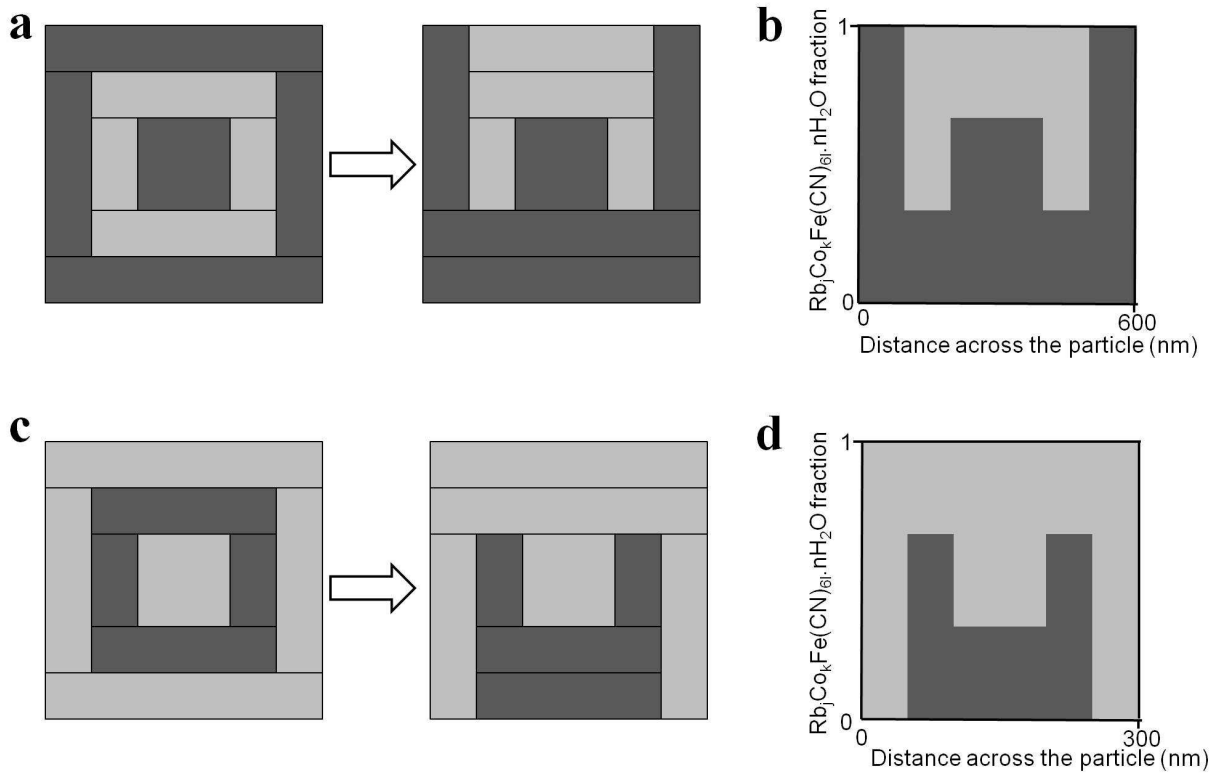

Figure S1. Scheme depicting calculation of the idealized cross-section mole fraction of the **BAB** and **ABA** type particles (a) and (c), respectively. The different colors represent the different compounds $Rb_aCo_bFe(CN)6_c{\cdot}mH_2O$ (dark grey) and $K_jNi_kCr(CN)_{6l}{\cdot}nH_2O$ (light grey). The calculation can be carried out using the measured layer thicknesses for individual particles.

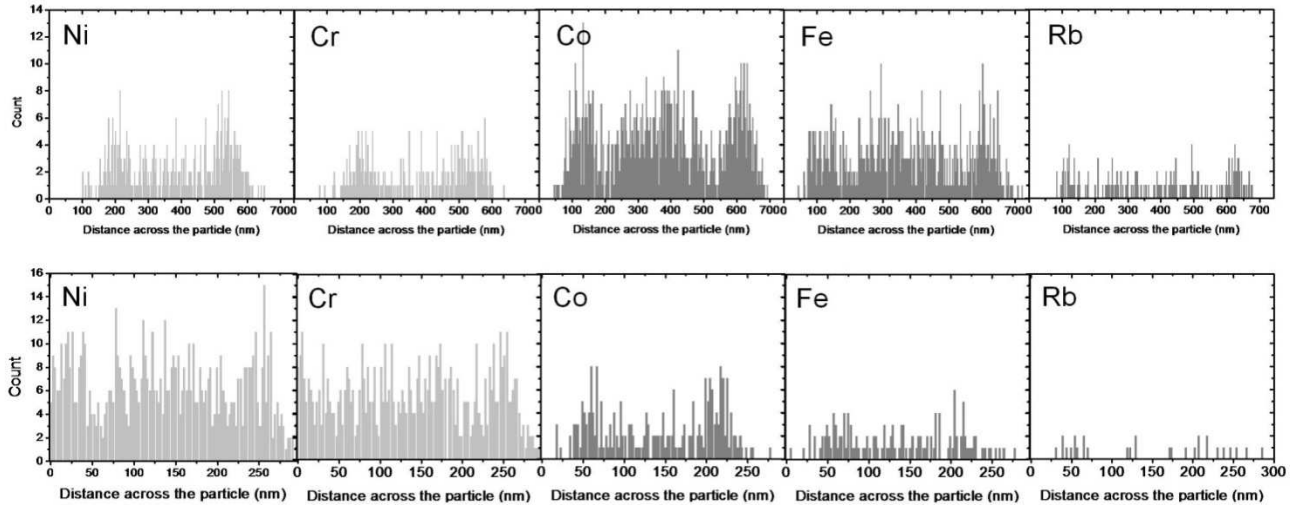

Figure S2. EDS line scans for RbCoFe-KNiCr-RbCoFe (**BAB**) (top) and KNiCr/RbCoFe/KNiCr (**ABA**) (bottom). Data are counts for each element detected against the position of the electron beam along the dashed line in Figure 1. The composite shown in Figures 1c and 1d in the text are generated by adding the contribution of iron, cobalt and rubidium normalized so that the sum of all measured elements equals 1.

2. Temporal response to irradiation at 40 K and high field magnetization at 2 K.

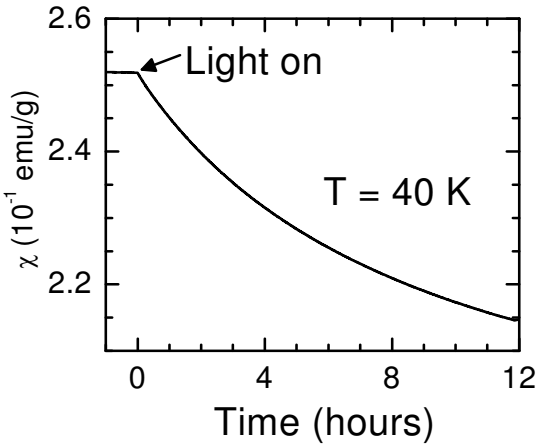

Figure S3. Magnetic susceptibility χ as a function of time in a **BA** heterostructure, with irradiation at T = 40 K. The light was turned on at time = 0.

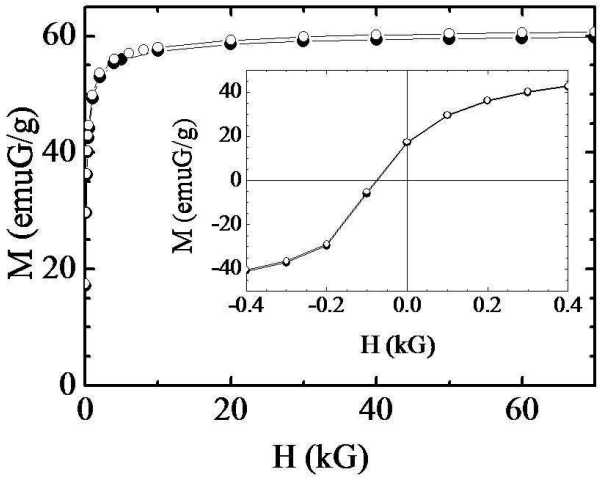

Figure S4. The magnetization, M, versus magnetic field, H, loops at 2 K for **BA**. The closed symbols are before irradiation and the open symbols are after photoexcitation but with the light off. The insets show an expanded region at low magnetic fields, the coercive fields, H_c, is 75 G.

3. Relative molar extinction coefficients and synthesis protocol.

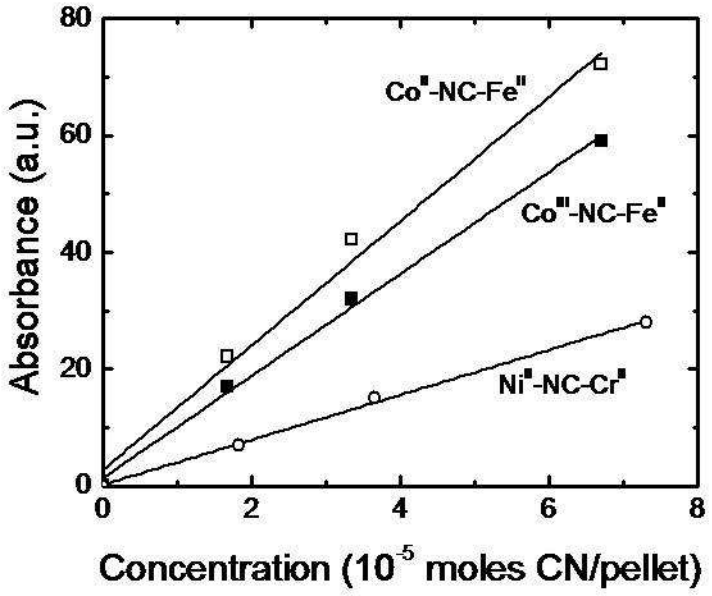

CN species	ω_0 (cm^{-1})	ε (A/mole CN)	Relative ε
Co^{II}-NC-Fe^{II}	2090	10.6×10^5	1
Co^{III}-NC-Fe^{II}	2120	8.7×10^5	0.82
Ni^{II}-NC-Cr^{II}	2170	3.8×10^5	0.35

Figure S5. IR absorbance of the C-N stretch associated with the bridging cyanide ligands as a function of concentration for Co^{III}-NC-Fe^{II} (LS), Co^{II}-NC-Fe^{II} (reduced) and Ni^{II}-NC-Cr^{III} pairs. Linear fits yielded relative molar extinction coefficients for the cyanide species within the compounds, where ω_0 is defined as the peak stretching frequency and ε is defined as the molar extinction coefficient.

For the molar extinction coefficient study, we synthesized pure $K_jNi^{II}_k[Cr^{III}(CN)6]_l \cdot nH_2O$ and $Rb_aCo^{II}_b[Fe^{III}(CN)_6]_c \cdot nH_2O$ in powder form. $K_jNi^{II}_k[Cr^{III}(CN)6]_l \cdot nH_2O$ is obtained by adding a solution of 75 mg of $K_3Cr(CN)_6$ in 10 mL H_2O to a solution of 50 mg $NiCl_2$ in 10 mL H_2O under vigorous stirring. $Rb_jCo^{II}_k[Cr^{III}(CN)_6]_l \cdot nH_2O$ is obtained by adding a solution of 75 mg of $K_3Fe(CN)_6$ in 10 mL H_2O to a solution of 50 mg $CoCl_2$ in 10 mL H_2O under vigorous stirring. The product is a deep purple precipitate. Both precipitates were collected by centrifugation and washed with 15 mL of water and 2×15 mL of acetone. The solutions were subsequently air-dried and pressed into a pellet following the method described in the experimental section. Consecutive solid-state dilution in KBr gives the range of concentrations used to determine the molar extinction coefficient.

4. FT-IR spectra.

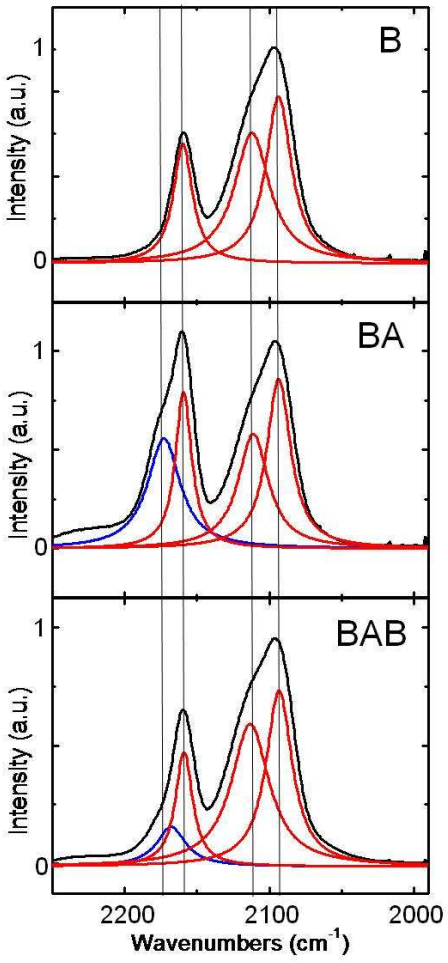

Sample B	xc(CoFe1)	2159.74	±0.07
	w(CoFe1)	15.99	±0.24
	A(CoFe1)	3.54	±0.04
	xc(CoFe2)	2111.94	±0.29
	w(CoFe2)	29.72	±0.66
	A(CoFe2)	7.19	±0.26
	xc(CoFe3)	2093.60	±0.13
	w(CoFe3)	21.61	±0.40
	A(CoFe3)	6.69	±0.22
Sample BA	xc(NiCr)	2172.86	±0.50
	w(NiCr)	27.51	±0.81
	A(NiCr)	4.82	±0.26
	xc(CoFe1)	2159.32	±0.12
	w(CoFe1)	13.67	±0.49
	A(CoFe1)	3.40	±0.20
	xc(CoFe2)	2111.06	±0.34
	w(CoFe2)	25.46	±0.85
	A(CoFe2)	4.65	±0.23
	xc(CoFe3)	2093.48	±0.16
	w(CoFe3)	20.11	±0.46
	A(CoFe3)	5.43	±0.20
SampleBAB	xc(NiCr)	2167.69	±1.89
	w(NiCr)	24.50	±1.56
	A(NiCr)	5.18	±1.42
	xc(CoFe1)	2158.97	±0.23
	w(CoFe1)	14.36	±0.81
	A(CoFe1)	8.77	±1.26
	xc(CoFe2)	2113.18	±0.25
	w(CoFe2)	31.83	±0.66
	A(CoFe2)	24.15	±0.77
	xc(CoFe3)	2093.23	±0.11
	w(CoFe3)	21.94	±0.36
	A(CoFe3)	20.52	±0.61

Figure S6. Room temperature FT-IR spectra for the RbCoFe core (**B**), RbCoFe/KNiCr (**BA**), and RbCoFe/KNiCr/RbCoFe (**BAB**) particles. All fits were performed using one, three or four Lorentzian lines (represented in blue for KNiCr and red for RbCoFe). On the right are the fitting parameters used for each sample, defining xc as the peak stretching energy, w as the peak half-maximum width, and A as the area under the curve. Note that the molar extinction coefficient of the Cr^{III}-CN-Ni^{II} CN stretch and the Fe^{III}-CN-Co^{II}(hs) CN are much smaller than those of the Fe^{III}-CN-Co^{II}(ls) and Fe^{II}-CN-Co^{II} CN stretches so the amount of these components appear smaller in the FTIR.

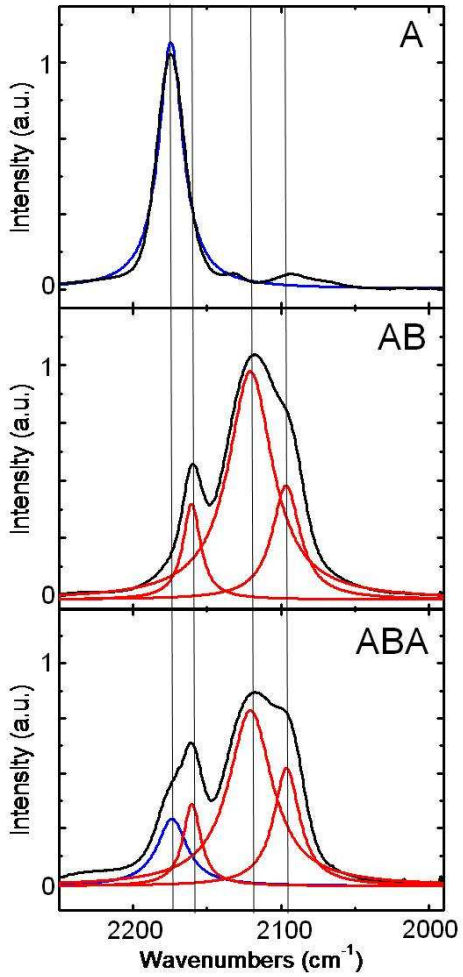

Sample A	xc(NiCr)	2174.51	±0.04
	w(NiCr)	19.92	±0.12
	A(NiCr)	20.47	±0.09
Sample AB	xc(CoFe1)	2160.39	±0.08
	w(CoFe1)	14.52	±0.33
	A(CoFe1)	7.57	±0.16
	xc(CoFe2)	2120.62	±0.14
	w(CoFe2)	36.43	±0.46
	A(CoFe2)	45.38	±0.78
	xc(CoFe3)	2096.51	±0.15
	w(CoFe3)	22.92	±0.55
	A(CoFe3)	14.27	±0.55
Sample ABA	xc(NiCr)	2173.65	±0.57
	w(NiCr)	24.64	±0.99
	A(NiCr)	4.73	±0.34
	xc(CoFe1)	2160.22	±0.21
	w(CoFe1)	14.63	±0.79
	A(CoFe1)	3.43	±0.30
	xc(CoFe2)	2120.62	±0.19
	w(CoFe2)	35.85	±0.65
	A(CoFe2)	18.01	±0.41
	xc(CoFe3)	2096.15	±0.14
	w(CoFe3)	21.24	±0.54
	A(CoFe3)	7.16	±0.28

Figure S7. Room temperature FT-IR spectra for the KNiCr core (**A**), KNiCr/RbCoFe (**AB**), and KNiCr/RbCoFe/KNiCr (**ABA**) particles. All fits were performed using one, three or four Lorentzian lines (represented in blue for KNiCr and red for RbCoFe). On the right are the fitting parameters used for each samples, defining xc as the peak stretching energy, w as the peak half-maximum width, and A as the area under the curve. On the AB sample, the The KNiCr signal is too weak to be fitted with satisfactory precision.

5. Magnetic susceptibility, χ, as a function of temperature for BAB, AB, and ABA particles

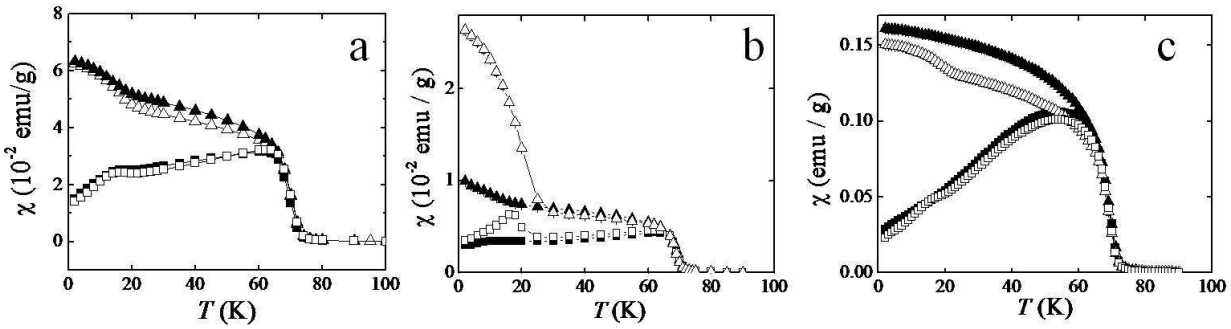

Figure S8. The field cooled magnetic susceptibility, χ, H=100G, as a function of temperature before irradiation (▲, "dark") and with the light off after 11 hours of irradiation with visible white light (Δ, "light"). a) RbCoFe / KNiCr / RbCoFe (**BAB**) particles b) KNiCr/RbCoFe (**AB**) particles, and c) KNiCr/RbCoFe/KNiCr (**ABA**) particles. The zero-field cooled light (□) and dark (■) states susceptibilities, χ, are also plotted.. Lines are guides for the eyes

7. TEM images of heterostructure.

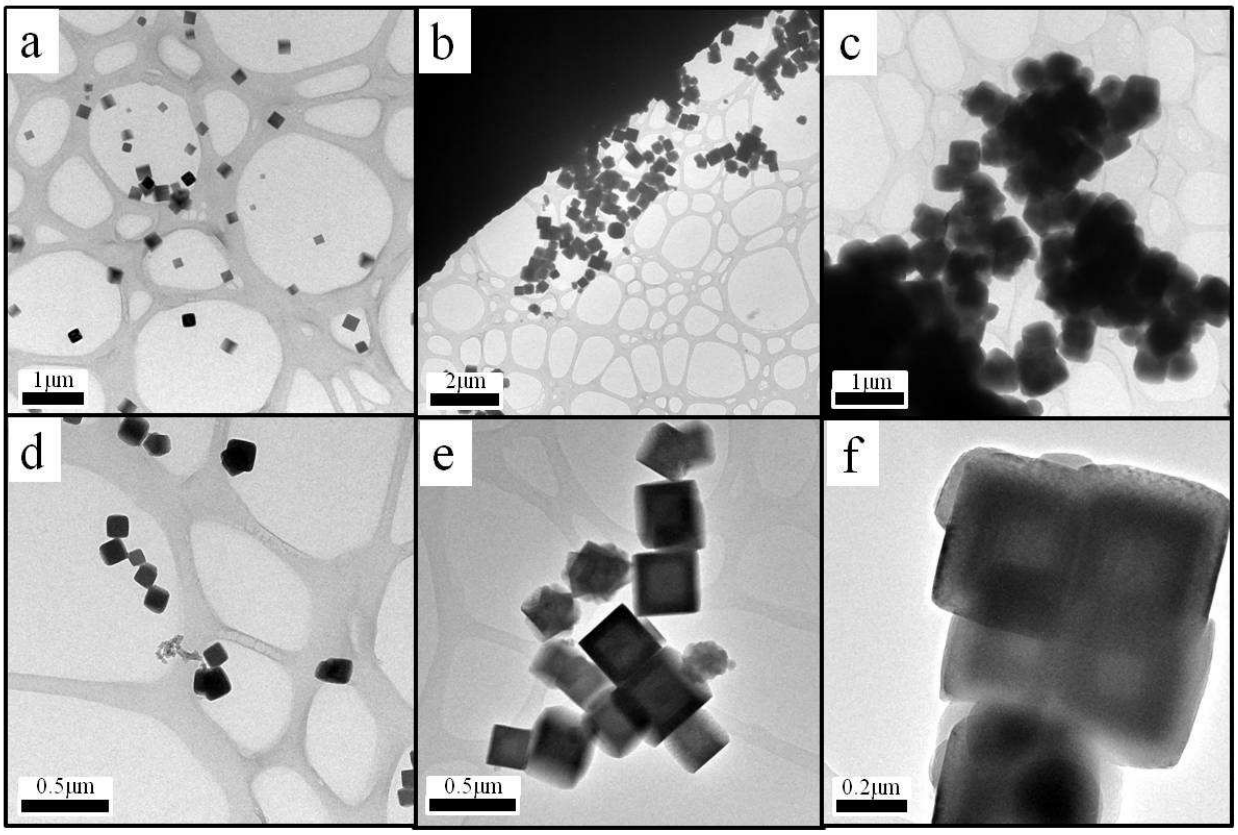

Figure S9. TEM picture of **A,** KNiCr core (a,d); the **AB,** KNiCr/RbCoFe core/shell particles (b, e); and the **ABA**, KNiCr/RbCoFe/KNiCr core/shell/shell particles (c, f). Some smaller, incomplete particles, likely due to side nucleation, appear in some images. Analysis of the TEM images shows that the total volume corresponding to these partially formed structures corresponds to 0.5-2.5 % of the total volume.

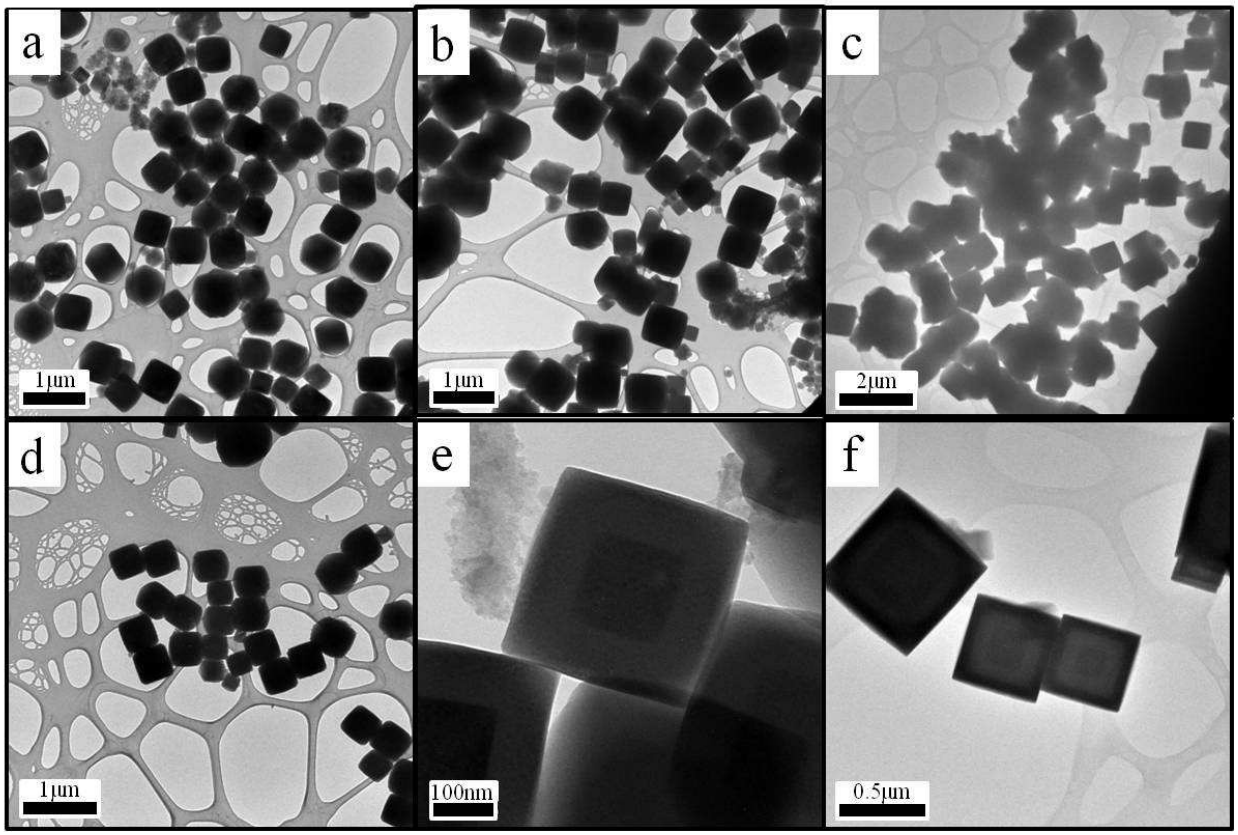

Figure S10. TEM picture of **B,** RbCoFe core (a,d); the **BA**, RbCoFe/KNiCr core/shell particles (b, e); and the **BAB**, RbCoFe/KNiCr/RbCoFe core/shell/shell particles (c, f).